Electrified Aircraft Trade-Space Exploration

Michael Kruger*, Saakar Byahut*, Alejandra Uranga†
University of Southern California, Los Angeles, CA 90089, U.S.A.

Aidan Dowdle‡, Jonas Gonzalez§, David K. Hall¶
Massachusetts Institute of Technology, Cambridge, MA 02139, U.S.A.

This work presents a design space exploration for electrified aircraft that use electrical components for propulsion, and identifies configurations and missions for which electrification can provide an energy-usage advantage relative to hydrocarbon-based propulsion. A framework was developed to capture the major trade-offs of electrification at cruise condition, as well as the effects of distributed propulsion and boundary layer ingestion. The analysis is based on a parametric exploration of the trade-space with focus on mission size (payload and range) and technology level. It considers aircraft classes ranging from a 20-passenger thin-haul up to a twin-aisle intercontinental transport. All-electric aircraft are found to be best at low ranges (200–500 nmi), requiring the lowest amount of on-board energy but with a limited feasibility region. Turbo-electric architectures can be beneficial even with current technology, and are best for long missions. Adding a turbo-generator to an electric aircraft, for a hybrid-electric propulsion system, acts as a range extender and is optimal for intermediate-size missions. Finally, leveraging distributed propulsion and boundary layer ingestion improves energy efficiency and expands the range of feasible missions for highly electrified aircraft.

I. Introduction

A. Motivation and Background

Commercial aircraft currently rely on hydrocarbons as the sole source of energy for propulsion. The variability of fuel prices, the growing emphasis on environmental sustainability, and the increased demand for air transportation have led to enhanced interest in fuel efficiency and emissions reduction for transport aircraft.

Aircraft propulsion system electrification has the potential to provide higher component efficiencies as well as lower emissions. Electrification, however, poses major challenges. The first is related to weight: although battery technology has improved substantially over the past decades, battery specific energy (energy per unit mass) is still orders of magnitude lower than that of hydrocarbon fuels. It is unclear whether the former can entirely replace the latter as the sole propulsive energy source.

In addition, directly replacing a conventional internal-combustion engine on an existing aircraft with an electric propulsion system is not expected to be beneficial due to the added complexity and weight.[1] To take advantage of electrification, the full aircraft needs to be reconfigured. Furthermore, electrification can facilitate the use of distributed propulsion (DP) and boundary layer ingestion (BLI) to increase performance.

Previous studies have shown benefits of electrification for transport aircraft by considering point-designs for a specific aircraft and propulsion architecture.[2–4] This paper presents a broad design-space exploration to address the challenges of electrification and highlight areas with potential. Using component models, technology levels, a unified view of propulsion system architectures, and a set of aircraft configurations and missions, we determine the areas favorable to electrification and the potential performance benefits.

*Graduate Student, Dept. of Aerospace and Mechanical Engineering, AIAA Student Member
†Gabilan Assistant Professor, Dept. of Aerospace and Mechanical Engineering, 854 Downey Way RRB 218, auranga@usc.edu, AIAA Senior Member
‡Graduate Student, Dept. of Electrical Engineering & Computer Science
§Graduate Student, Dept. of Aeronautics and Astronautics
¶Research Engineer, Dept. of Aeronautics and Astronautics, AIAA Member.

B. Potential Benefits of Electrification

The use of an electrified propulsion system might have several advantages compared to a conventional hydrocarbon-based, mechanically-linked system. A direct benefit is achieved from higher component efficiencies. Furthermore, distributing power from a source to a large number of propulsor units is simpler when done electrically via wires and electric motors, as opposed to mechanically via shafts and gears. Thus, electrification facilitates the use of distributed propulsion, which in turn facilitates boundary layer ingestion. We now briefly present the benefits of electrification related to conversion efficiency, boundary layer ingestion, and distributed propulsion.

1. Source to Load Conversion Efficiency

Electrified propulsion systems can convert electrical energy into useful propulsive power more efficiently than conventional systems. This is evident in the chain of efficiencies from energy source to propulsor (fan or propeller). With current turbofan and turboprop engines, the overall efficiency is of the order of 30% to 40%, with a major part of the losses coming from gas turbines, with a thermal efficiency of 50% or less. For an all-electric, battery-powered propulsion system, the efficiencies of the electrical components in the chain (motors and power electronics) can give an overall efficiency from source to propulsor of around 70% or more.[5]

Even if the propulsion system is only partly electrified, the higher electrical component efficiencies can be exploited with hybrid-electric and turbo-electric propulsion system architectures. As electrical components improve, their efficiencies are expected to reach upwards of 99%,[6,7] further improving the system-level efficiency of electrified propulsion systems.

2. Boundary Layer Ingestion (BLI)

In a conventional engine installation, the propulsors are mounted away from the airframe. They ingest uniform freestream flow and their jets counteract the momentum defect in the airframe wake. At cruise, the jets and wakes combine to a zero net momentum (thrust equals drag), but both the airframe wake and the propulsor jet represent wasted kinetic energy, as illustrated in Fig. 1. A more efficient alternative is to place the propulsors in the boundary layer of the airframe, thus re-energizing the slower-moving flow which otherwise forms the wake. The resulting combined wake and jet has lower kinetic energy and lower losses than a conventional propulsor.

The process of having at least part of the airframe boundary layer ingested by the propulsion system is called boundary layer ingestion (BLI), which is known[8–10] to increase the overall efficiency of the aircraft. The benefits of BLI come from four sources: (i) reduced propulsor jet dissipation and corresponding increased propulsive efficiency; (ii) reduced wake dissipation as the propulsors partially eliminate the wake; (iii) reduced surface dissipation due to generally smaller embedded nacelles with lower surface velocities; and (iv) reduced aircraft weight thanks to the smaller nacelles and engines, which in turn enables smaller and lighter wings.

The level of benefit that BLI provides relative to a conventional engine installation is a function of the amount of boundary layer ingested. The optimal case is when all of the body's boundary layer is ingested, but achieving full ingestion requires that the propulsor system inlets cover all of the airframe trailing edges (including fuselage, wings, and tails). This can be difficult to realize in practice, especially if only a small number of large propulsors are to be used.

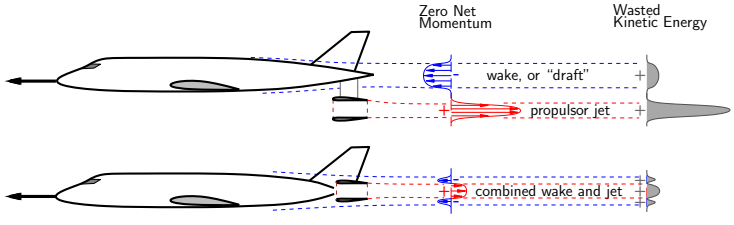

Figure 1: Illustration of the aerodynamic benefit of boundary layer ingestion.[8]

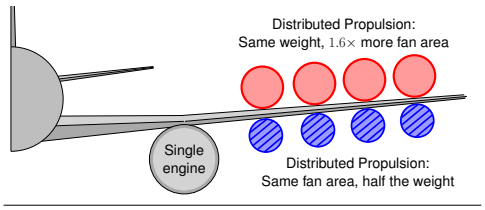

Figure 2: Illustration of weight reduction benefits of distributed propulsion.

One way to increase BLI is use of distributed propulsors, which is much easier to achieve when power is distributed to the propulsors electrically, rather than mechanically via shafts. It is thus reasonable to assume that electrification facilitates BLI.

3. Distributed Propulsion

In addition to helping increase boundary layer ingestion, distributed propulsion (DP) can provide a weight reduction benefit. This can be seen by considering the relation between the propulsor mass and the mass flow through it. The mass of a propulsor, m_{prop}, to first order, can be assumed to scale with its volume and hence with the cube of the characteristic length, while the propulsor mass flow, $\dot{m}_{\text{prop}}$, scales with its frontal area, represented by a characteristic length squared. Thus, the mass of a propulsor and its mass flow rate are linked by a cube-squared relationship:

$$m_{\text{prop}} \sim \dot{m}_{\text{prop}}^{3/2} . \tag{1}$$

The thrust-to-weight ratio thus decreases with $\dot{m}_{\text{prop}}^{3/2}$. As an example, consider the use of four small DP units instead of a large one as illustrated in Fig. 2. If the single large propulsor is replaced by the DP system with the requirement of same total thrust, then for the same total fan area, the weight would be reduced by half (mass factor of square-root of the number of propulsors). If instead, the requirement is to maintain the same propulsion system weight, the four-unit DP system would provide 1.6 times more total fan face area (mass flow factor of cubic root of the number of propulsors), enabling reduced fan pressure ratio and increased propulsive efficiency.

The use of a distributed propulsion system thus has the advantage of being lighter or more efficient, and the larger the number of propulsors the better—at least in principle. As mentioned previously, it is easier to distribute power to a large number of propulsors via an electrical link than a mechanical one. Thus, electrification facilitates DP and can result in a weight-saving benefit.

C. Terminology

Throughout this work, the term *conventional* is used to refer to a propulsion system architecture that uses hydrocarbon fuel as the sole source of energy and includes no electrical components for propulsion. A *turbo-electric* architecture refers to a propulsion system that retains the hydrocarbon fuel as the sole energy source, but employs electrical components in the conversion from source to load: one or more gas turbines generate power that is distributed to one or more fans through a component chain of a generator, converter, and motor. In a *fully turbo-electric* architecture, all the fans are electrically driven, whereas a *partial turbo-electric* design has both electrically and mechanically driven fans.

A *hybrid-electric* architecture relies on both batteries and hydrocarbon fuel to store energy for propulsion. Hybrid-electric architectures could be further classified as either *series* or *parallel*. In series, the propulsors receive only electrical power from the turbo-generator and the battery, whereas in parallel, the mechanical fans receive additional power from a battery-powered motor mounted on the same shaft as the turbine. Finally, in an *all-electric* architecture all the energy needed for propulsion is stored in batteries.

The term "*electrified*" is used to refer to a propulsion system that uses electrical components to generate thrust. It therefore encompasses turbo-electric, hybrid-electric and all-electric architectures.

D. Scope

In the present work, a conceptual-level framework is developed based on a generalized range equation, which ties together modules for aircraft sizing, power balance, and propulsion system. The propulsion system model uses a unified view in which all the architectures, from conventional to all-electric, are represented via a simple parametric load and source representation. We determine the missions (range and payload), aircraft configurations, and propulsion architectures for which an electrified aircraft has a potential energy-usage advantage relative to conventional aircraft. It captures the effects due to weight trade-offs, boundary layer ingestion, distributed propulsion, electrification level, and technology level.

II. Methodology

In this section, we start by identifying the metrics used to quantify the level of electrification and to determine the performance of a particular conceptual aircraft. An overview of the analysis framework is provided, followed by a unified description of propulsion system architectures. Each of the modules that compose the framework is then presented in detail. Finally, the technology assumptions used in the present study are introduced, followed by a description of aircraft and missions that serve as baselines for the analysis.

A. Metrics

1. *Electrification Level*

The propulsion system is parameterized based on power split at the source and the load. The source electrification factor, f_S, quantifies the fraction of power supplied by batteries (electrical source), P_{bat}, versus that supplied by hydrocarbon fuel (mechanical source), P_{turb}. It is defined as

$$f_S = \frac{P_{\text{bat}}}{P_{\text{bat}} + P_{\text{turb}}} \ , \tag{2}$$

where the denominator is the total power used throughout the mission. Conventional and turbo-electric aircraft have $f_S = 0$, hybrid-electrics have f_S between 0 and 1, and all-electrics have $f_S = 1$.

Useful power on the load end is quantified by the mechanical flow power delivered by the propulsors, P_K, defined based on the power balance method.[11] Electrification at the load relates the flow power delivered via mechanically-driven propulsors (mechanical load), P_{K_M}, and via electrically-driven propulsors (electrical load), P_{K_E}. The load electrification factor is defined as

$$f_L = \frac{P_{K_E}}{P_{K_E} + P_{K_M}} \ , \tag{3}$$

where the denominator represents total power required by the propulsors during a mission. A conventional aircraft has $f_L = 0$, since all the flow power is mechanical. Partial turbo-electric and hybrid aircraft have f_L between 0 and 1. Fully turbo-electric and all-electric aircraft have $f_L = 1$. Thus, load electrification distinguishes between partial and fully turbo-electric, as well as between hybrid- and all-electric architectures.

The entire design space of electrified propulsion architectures can be described by the two parameters f_S and f_L, providing a unified view of the propulsion system.

2. *Performance*

The performance metric chosen is the productivity-specific energy consumption, defined as the mission energy per payload mass per unit range

$$\text{PSEC} = \frac{m_{\text{fuel}}\, h_{\text{fuel}} + m_{\text{bat}}\, \text{BSE}}{m_{\text{PL}}\, R} \ , \tag{4}$$

where m_{fuel}, m_{bat}, and m_{PL} are the masses of the fuel, battery[a], and the payload respectively; $h_{\text{fuel}} = 43\,\text{MJ/kg}$ is the specific energy of hydrocarbon fuel; BSE is the battery specific energy; and R is the mission range. Thus, PSEC is a measure of the on-board energy required to bring passengers from point A to point B, and accounts for how efficiently the energy is used to perform that mission.

B. Propulsion Architectures

1. *Unified View*

The unified view of the propulsion system is illustrated in Fig. 3. The left end shows the energy sources: hydrocarbon fuel and battery. From these, power flows to the load on the right end of the figure, comprised of mechanically- and/or electrically-driven propulsors (typically ducted fans). When a fan is powered by a turbine via a shaft, the propulsor is referred to as mechanically powered. When a fan is powered by a motor (either via a battery or a turbine+generator), the propulsor is electrically powered. An architecture is defined by the specification of f_S and f_L, each of which is set to a value between 0 and 1.

[a]When a battery is on board, it is assumed to be fully charged at takeoff.

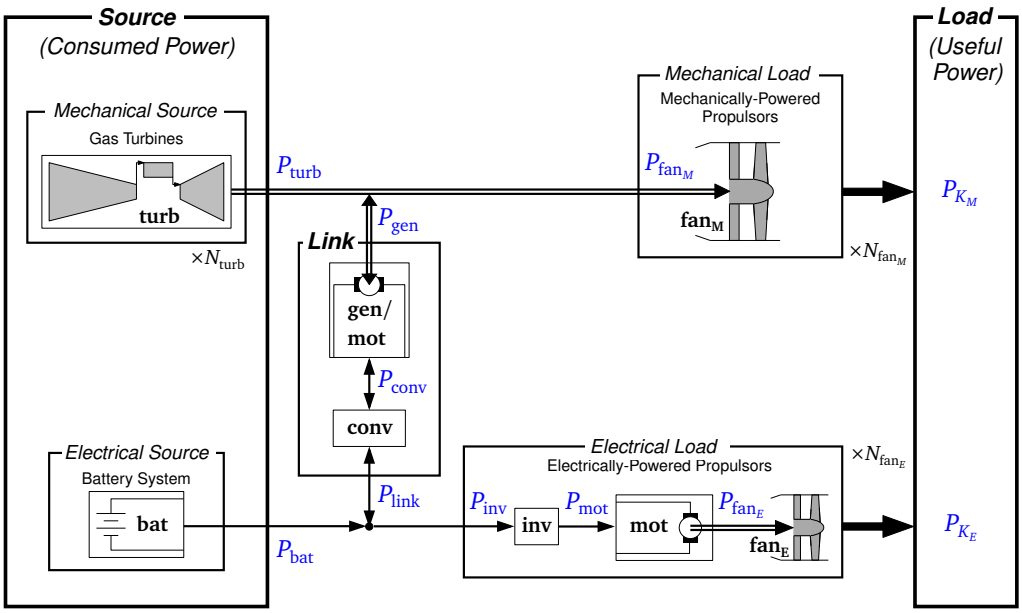

Figure 3: Propulsion system architectures unified model.

Table 1: Propulsion system architectures represented by the unified view and their defining parameters: load and source electrification factors, f_S and f_L.

f_L \ f_S	0	$(0,1)$	1
0	Conventional	Parallel Hybrid	All-electric
$(0,1)$	Partial Turbo-electric	Series/Parallel Partial Hybrid	All-electric
1	Fully Turbo-electric	Series Hybrid	All-electric

When a zero value is used for one of the factors, the corresponding component is massless and is thus removed from the system. For instance, if $f_S = 0$, no batteries are carried on board. If $f_L = 0$, there are no electrically-driven fans. A combined $f_S = 0$ and $f_L = 0$ represents a conventional aircraft. The specific values of (f_S, f_L) that define each particular architecture are given in Table 1.

This unified propulsion system model has mechanical and electrical sub-systems, shown on the top and bottom portions of Fig. 3 respectively, optionally linked via a generator. The mechanical part consists of sets made of one gas turbine connected to one mechanically-powered propulsor via a shaft. There can be N_{fan_M} sets. For a conventional aircraft, this is the entire propulsion system, and usually, N_{fan_M} is one or two. The electrical part consists of a battery system (essentially a large battery pack) connected to an inverter that provides power to N_{fan_E} motors, each in turn driving one fan. For an all-electric architecture (f_S and f_L both set to 1), the top half is removed and there is no generator to function as a link. The level of distribution for a distributed propulsion system is characterized by the number of fans, N_{fan_E}.

2. Power Flow in Different Architectures

A turbine can be used to send power via an electro-mechanical conversion link to the electrical part, for either recharging the batteries or distributing power to a range of electrical motors+fans. In this scenario, the electrical machine in the link functions as a generator and power flows from top to bottom sub-parts in the figure. Conversely, a battery can be used to augment the power to a mechanically-driven fan, in which case power flows from bottom (electrical) to top (mechanical) parts, and the link functions as motor. Thus, the sub-systems are connected by an electrical machine that can transfer power in both directions.

For turbo-electric architectures, gas turbines power both mechanically-driven propulsors and the generator (partial turbo-electric) or just the generator (fully turbo-electric). In either case, the generator drives

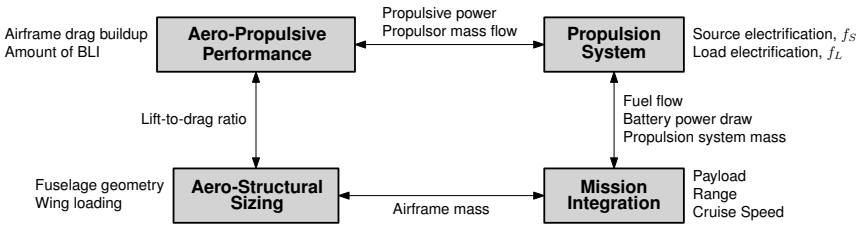

Figure 4: Framework overview: modules and their interactions.

motors and electrically-driven propulsors, and there is no battery ($f_S = 0$). Since there are no mechanically-driven propulsors in a fully turbo-electric architecture, $f_L = 1$.

For hybrid-electric architectures, both the gas turbine and the battery provide energy. All parts of the model are activated, and f_S and f_L both vary between 0 and 1.

C. Framework

1. *Overview*

A modular approach is taken to size and integrate an aircraft with its components, and evaluate its performance over a given mission. The aircraft model consists of four modules, as shown in Fig. 4.

Each module "builds up" a part of the aircraft based on the mission requirements or constraints. The propulsion system takes into account whether the architecture is conventional or electrified, and the amount of distribution, to determine the mass and size of its components. The mission integration module takes the mission requirements of payload, range, and cruise speed, and uses a generalized range equation to calculate takeoff mass, power required, *etc.* The airframe mass is calculated from the mass buildup in the aero-structure module. The aero-propulsive performance module determines the drag and includes the effects of boundary layer ingestion (BLI). These modules are described in detail in this section.

The bi-directionality of the arrows in Fig. 4 indicates that information flows both ways between modules. The modules are integrated into our design framework using the GPKit geometric programming optimization tool,[12] with mission energy PSEC as the objective function[b]. For a given technology level, mission requirements, amount of BLI and distribution, the framework thus produces an aircraft that minimizes the onboard energy as quantified by PSEC.

In what follows, we detail the equations that constitute the framework that was developed for the trade-space exploration.

2. *Mission Integration*

The flight mission is modeled as a constant-speed cruise segment only. With conventional and turbo-electric architectures, all the energy used for propulsion comes from fuel. As fuel is burned, the aircraft mass, m, changes at a rate equal to the fuel mass flow rate, $\dot{m}_{\text{fuel}}$, such that $-\mathrm{d}m/\mathrm{d}t = \dot{m}_{\text{fuel}}$ where the minus sign reflects the convention that $\dot{m}_{\text{fuel}}$ is positive and m decreases over time, or equivalently

$$-\frac{\mathrm{d}m}{m} = \frac{\dot{m}_{\text{fuel}}}{m}\,\mathrm{d}t\ . \tag{5}$$

While $\dot{m}_{\text{fuel}}$ is not constant throughout the mission[c] we can assume that $\dot{m}_{\text{fuel}}/m$ is constant—which is equivalent to assuming a constant specific thrust. The above equation can thus be integrated along the mission to get

$$\frac{m_{\text{init}}}{m_{\text{final}}} \;=\; \exp\left(\frac{\dot{m}_{\text{fuel}}}{m}\,\Delta t\right)\ , \tag{6}$$

where m_{init} and m_{final} are the initial (take-off) and final (landing or zero-fuel) aircraft masses, and Δt is the total flight time. The fuel mass m_{fuel} is related to initial and final masses by $m_{\text{init}} = m_{\text{final}} + m_{\text{fuel}}$, and for

[b]Using GPKit allows us to specify the problem as a set of variables and constraints. GPKit then solves the problem by minimizing PSEC, returning the values for the variables of the optimal design and their sensitivities.

[c]The thrust level and $\dot{m}_{\text{fuel}}$ change along the mission to maintain a constant speed as the aircraft mass decreases.

a mission at constant flight speed V_∞ the range is $R = \Delta t\, V_\infty$, such that

$$\frac{m_{\text{fuel}}}{m_{\text{final}}} \;=\; \exp\left(\frac{\dot{m}_{\text{fuel}}}{m}\,\frac{R}{V_\infty}\right) - 1 \;. \tag{7}$$

This is just an alternative form of the Breguet range equation[d].

For a hybrid-electric aircraft, the battery energy consumption must also be modeled. An additional equation relates the power supplied to the battery to the battery energy used. The battery energy, E_{bat}, is the energy supplied by the battery during the mission and derived by integrating the battery power, $\dot{E}_{\text{bat}}$, over the flight time. When the time integral is changed to a mass integral using Eqn. (5), it is found that

$$E_{\text{bat}} = \frac{\dot{E}_{\text{bat}}}{\dot{m}_{\text{fuel}}}\left(m_{\text{init}} - m_{\text{final}}\right) \;. \tag{8}$$

Using Eq. (6) to write m_{final} in terms of m_{init}, the battery energy can be expressed as

$$E_{\text{bat}} \;=\; \frac{\dot{E}_{\text{bat}}\, m_{\text{init}}}{\dot{m}_{\text{fuel}}}\left[1 - \exp\left(-\frac{\dot{m}_{\text{fuel}}}{m}\,\frac{R}{V_\infty}\right)\right] \;. \tag{9}$$

E_{bat} is the total *usable* energy stored in the battery at take-off and $\dot{E}_{\text{bat}}$ is the instantaneous battery-supplied power, under the assumption that $\dot{E}_{\text{bat}}/m$ is constant. The battery mass is assumed to stay constant.

The all-electric is a special case since all energy comes from batteries and the aircraft mass stays constant. Flight time is determined by the rate at which the battery energy is used, and range is then simply estimated as

$$R \;=\; V_\infty\, \Delta t \;=\; V_\infty\, \frac{E_{\text{bat}}}{\dot{E}_{\text{bat}}} \;, \tag{10}$$

where again $\dot{E}_{\text{bat}}$ is a mission-averaged power value.

3. Aero-Structural Sizing

The aircraft take-off mass is the sum of the masses of the payload, fuel, airframe, and propulsion system. The payload mass is specified as part of the mission definition. The fuel mass is an output calculated for each case considered. The propulsion system mass is determined as part of the propulsion system module (to be described later).

The aero-structural sizing module specifies the airframe structural mass. The airframe is broken down into the wing, horizontal tail, vertical tail, fuselage, landing gear, and miscellaneous mass contributions as

$$m_{\text{AF}} = m_{\text{wing}} + m_{\text{HT}} + m_{\text{VT}} + m_{\text{fuse}} + m_{\text{gear}} + m_{\text{misc}} \;. \tag{11}$$

The sub-component masses are estimated based on empirical factors as follows. The wing mass depends on wing reference area and span, and is calculated as

$$m_{\text{wing}} = K_{\text{wing}}\frac{S_{\text{wing}}^2}{b} \;. \tag{12}$$

The masses for vertical tail, horizontal tail, and fuselage scale with the respective wetted areas,

$$m_{\text{HT}} = K_{\text{HT}}\, S_{\text{HT}} \quad , \quad m_{\text{VT}} = K_{\text{VT}}\, S_{\text{VT}} \quad , \quad m_{\text{fuse}} = K_{\text{fuse}}\, S_{\text{fuse}} \;. \tag{13}$$

The surfaces for the tails are calculated from specified tail volume coefficients. The landing gear and miscellaneous equipment are assumed to depend on take-off weight as

$$m_{\text{gear}} = K_{\text{gear}}\, m_{\text{init}} \quad , \quad m_{\text{misc}} = K_{\text{misc}}\, m_{\text{init}} \;. \tag{14}$$

The K-factors are scaling parameters that are taken from Raymer[13] when considering a thin-haul aircraft, and correlated to TASOPT[14] results for larger aircraft.

[d]The range equation is usually written as $R = \frac{L}{D}\,\frac{V_\infty}{g}\,\frac{1}{SFC}\,\ln\left(\frac{m_{\text{init}}}{m_{\text{final}}}\right)$. Since $SFC = \dot{m}_{\text{fuel}}/T$, and at cruise $L{=}W{=}m\,g$ and $D{=}T$, the range equation becomes $R = \frac{m}{\dot{m}_{\text{fuel}}}\,V_\infty\,\ln\left(\frac{m_{\text{fuel}}}{m_{\text{final}}} + 1\right)$ which is equivalent to Eqn. (6).

Table 2: Structural and aerodynamic scaling parameters.

	K_{wing} [kg/m^3]	K_{HT} [kg/m^2]	K_{VT} [kg/m^2]	K_{fuse} [kg/m^2]	K_{gear} [-]	K_{misc} [-]	K_{LD} [-]
Thin-haul	9.8	9.8	9.8	6.8	0.057	0.1	9.5
Larger classes[a]	17.9	26.7	31.7	34.3	0.053	0.01	15.2

[a]The various aircraft classes considered in this study are introduced in Section II.E

The lift-to-drag ratio for the baseline aircraft in the absence of BLI is calculated from Raymer[13] as

$$\frac{L}{D} = K_{\text{LD}} \frac{\sqrt{AR\, S_{\text{wing}}}}{S_{\text{wet}}} , \tag{15}$$

where K_{LD} is a scaling factor, AR the wing aspect ratio, and S_{wet} the total aircraft wetted surface.

Table 2 lists the various scaling parameters from this section used in the current work.

4. Propulsion System

At the system level, the propulsion system is characterized by its power and its mass. A thermal management system is included to handle the heat rejected by each component.

Power

The power levels at the individual junctions of the unified propulsion system are labeled in Fig. 4, and the power analysis is done based on the power balance method.[11] The total mechanical power delivered to the flow by the propulsion system is

$$P_K = P_{K_M} + P_{K_E} , \tag{16}$$

where P_{K_M} and P_{K_E} are the mechanical powers delivered to the flow by the mechanically- and electrically-driven propulsors respectively. Denoting by N_{fan_E} and N_{fan_M} the number electrical and mechanical propulsors, respectively, the flow powers are given by

$$P_{K_E} = N_{\text{fan}_E}\, \eta_{\text{fan}}\, P_{\text{fan}_E} \tag{17}$$

$$P_{K_M} = N_{\text{fan}_M}\, \eta_{\text{fan}}\, P_{\text{fan}_M} , \tag{18}$$

where P_{fan_E} and P_{fan_M} are the per-propulsor shaft powers, and η_{fan} is the fan efficiency, assumed to be the same for all fans.

The non-dimensional relationship between battery efficiency, η_{bat}, and power, P_{bat}, is given by the Ragone relation:[15]

$$\frac{P_{\text{bat}}}{P_{\text{max}}} = 4\, \eta_{\text{bat}}\, (1 - \eta_{\text{bat}}) , \tag{19}$$

where P_{max} is the maximum power that the battery can deliver. This efficiency exists because of losses inside the battery and has the effect that the usable amount of energy effectively decreases as the battery is operated at higher power levels. When E_{tot} and P_{max} are divided by the battery mass, battery specific energy (BSE) and battery specific power (BSP) are obtained, both of which are important technology parameters to be discussed in Section II.D.

Down the electrical chain, each electrical propulsor is assumed to be driven by a motor of efficiency η_{mot}, and an inverter[e] of efficiency η_{inv}. We denote by P_{mot} the power delivered to the motor by the inverter, and P_{inv} the power delivered to the inverter, such that

$$P_{\text{fan}_E} = \eta_{\text{mot}}\, P_{\text{mot}} \tag{20}$$

$$P_{\text{mot}} = \eta_{\text{inv}}\, P_{\text{inv}} . \tag{21}$$

The power that reaches the inverters comes from the battery system and possibly from the mechanical source via the electro-mechanical energy-conversion link, *i.e.*,

$$N_{\text{fan}_E}\, P_{\text{inv}} = P_{\text{bat}} + P_{\text{link}} . \tag{22}$$

[e]In this work, any converter (inverter or rectifier) is assumed to include a controller.

On the mechanical side, hydrocarbon fuel is burned at a rate $\dot{m}_{\text{fuel}}$ to drive N_{turb} gas turbines. Denoting by P_{turb} the power output of each turbine, η_{th} their thermal efficiency, and $h_{\text{fuel}} = 43\,\text{MJ/kg}$ the jet fuel specific energy, the total power out of the mechanical source system is

$$N_{\text{turb}}\, P_{\text{turb}} \;=\; \eta_{\text{th}}\, h_{\text{fuel}}\, \dot{m}_{\text{fuel}} \;. \tag{23}$$

It is assumed that there are as many turbines as there are mechanically-driven fans, *i.e.*, $N_{\text{turb}} = N_{\text{fan}_M}$.

Finally, power may be directed from the mechanical source towards the electrical load, such that at the top junction of the electro-mechanical energy-conversion link we have

$$N_{\text{turb}}\, P_{\text{turb}} \;=\; P_{\text{gen}} \;+\; P_{\text{fan}_M} \;, \tag{24}$$

where P_{gen} is the power sent down to the generator. The amount of power P_{link} that exits the link, and which may be used to recharge the batteries in addition or instead of driving the electrical fans, depends on the converter efficiency η_{conv} and the generator efficiency η_{gen}, and is such that

$$P_{\text{link}} = N_{\text{turb}}\, \eta_{\text{conv}}\, P_{\text{conv}} \tag{25}$$

$$P_{\text{conv}} = \eta_{\text{gen}}\, P_{\text{gen}} \;. \tag{26}$$

Note that when power flows upwards from the electrical part towards the mechanical part, the powers P_{link}, P_{conv}, P_{gen} will be negative.

Thermal Management

Each electrical component is assumed to dissipate heat at a rate $\dot{Q}$, which must be removed via the thermal management system (TMS). The total dissipated heat is

$$\dot{Q} \;=\; N_{\text{fan}_M} \left(\dot{Q}_{\text{gen}} + \dot{Q}_{\text{rect}} \right) \;+\; N_{\text{fan}_E} \left(\dot{Q}_{\text{inv}} + \dot{Q}_{\text{mot}} \right) \;+\; \dot{Q}_{\text{bat}} \;, \tag{27}$$

where the heat dissipation of each component is determined by its power throughput and efficiency as

$$\dot{Q}_{(\cdot)} = \left(1 - \eta_{(\cdot)}\right) P_{(\cdot)} \;. \tag{28}$$

For instance, $\dot{Q}_{\text{mot}} = (1-\eta_{\text{mot}})\, P_{\text{mot}}$. The gas turbines are assumed to include their own thermal management system, which is accounted for in the turbine mass.

Mass

The overall propulsion system mass is equal to the sum of its component masses, namely

$$m_{\text{prop}} \;= N_{\text{fan}_M} \left(m_{\text{turb}} + m_{\text{gen}} + m_{\text{conv}} + m_{\text{fan}_M} + m_{\text{nace}_M} \right) \tag{29}$$

$$+\; N_{\text{fan}_E} \left(m_{\text{inv}} + m_{\text{mot}} + m_{\text{fan}_E} + m_{\text{nace}_E} \right) \;+\; m_{\text{TMS}} \;. \tag{30}$$

The masses of the turbines and fans (mechanically- and electrically-driven) are calculated from their respective mass flows following the cube-squared law, namely

$$m_{\text{turb}} = K_{\text{turb}}\, \dot{m}_{\text{turb}}^{1.2} \quad , \quad m_{\text{fan}} = K_{\text{fan}}\, \dot{m}_{\text{fan}}^{1.2} \;. \tag{31}$$

In the current work values of $K_{\text{turb}} = 45.6$ and $K_{\text{fan}} = 1.3$ are used (derived from TASOPT results[14]), with the units for the coefficients as required to give dimensions of mass in the product. Initially, a cube-squared scaling was used, but an exponent of 1.2 was found to give a better fit to existing TASOPT data.

The generator, converter, inverters, and motors are assumed to have constant power densities, so their masses are determined from an assumed power-to-mass ratio $\left[\frac{P}{m}\right]$ as

$$m_{(\cdot)} = P_{(\cdot)} \left[\frac{P}{m} \right]_{(\cdot)}^{-1} \;. \tag{32}$$

Nacelle masses are assumed to scale linearly with the propulsor mass flow as

$$m_{\text{nace}_{M/E}} = K_{\text{nace}} \dot{m} \;, \tag{33}$$

where a value of $K_{\text{nace}} = 4.56$ s was used in the current work.

The TMS size scales with the heat flow, again via a power-to-mass ratio, so its mass is

$$m_{\text{TMS}} = \dot{Q} \left[\frac{P}{m}\right]^{-1}_{\text{TMS}} . \tag{34}$$

The power density values are set based on the technology level as given in Table 3.

The mass of the wires are not explicitly included, but are assumed to be accounted for in the masses of the individual components. Power distribution wiring strongly depends on the aircraft configuration, and the placement of the different components within the airframe. Such level of detail is beyond the scope of the present framework and trade-space analysis.

5. Aero-Propulsive Performance

In an aircraft configuration with boundary layer ingestion, the performance of the propulsion system and that of the airframe cannot be clearly differentiated, as the notions of thrust and drag become ambiguous. In order to address this difficulty and estimate the performance of both BLI and non-BLI aircraft, the power balance method, introduced by Drela,[11] is employed here. In particular, we relate the performance of an aircraft with BLI to that of a non-BLI aircraft by building upon previous BLI analyses papers.[8,10]

In order to represent the effects of BLI, a number of equations and constraints must be included in the framework. This includes relations between flow power, non-BLI configuration drag, and propulsor mass flow. Additionally, specifications for engine size (fan and nacelle) are needed.

As mentioned previously, the benefit of BLI depends on the level of ingestion, which is quantified by the ingestion fraction f_{BLI}: the fraction of airframe's boundary layer kinetic energy defect ingested by propulsors. In what follows, a prime $(\,)'$ denotes quantities of a non-BLI configuration.

For this application, the relationships reduce to

$$\sum_i \dot{m}_i (V_{\text{jet},i} - V_\infty) = D' \left(1 - \sum_i f_{\text{BLI},i} \left(\frac{D'_p}{D'}\right)\right) \tag{35}$$

$$P_{K,i} = \frac{1}{2}\,\dot{m}_i\,(V_{\text{jet},i}^2 - V_\infty^2) + f_{\text{BLI},i}\,f_{\text{surf}}\,D'_p\,V_\infty \tag{36}$$

Equation 35 is the power balance equation, as presented by Hall,[10] where the propulsive power terms on the left hand side balance the power dissipation terms on the right. The summations account for multiple propulsion streams. Here, they are simplified into two streams, one from mechanically-driven propulsors and one from electrically-driven propulsors. Equation 36 defines the mechanical powers delivered to the flow by each of the streams. These powers directly size the propulsion system and consist of the change in flow kinetic energy and the re-energizing of the ingested boundary layer.

These equations also show the dependence of BLI benefit on propulsion integration and airframe parameters. The non-BLI total aircraft drag, D', directly scales the change in freestream velocity, V_∞, and in turn the flow power. The boundary layer ingestion fraction, f_{BLI}, reduces the jet velocity, $V_{\text{jet},i}$. Although f_{BLI} contributes directly to the power requirement, greater BLI ultimately reduces the overall power. The ingestible profile drag fraction, D'_p/D', scales the BLI benefit since the energy defect of some drag components (such as induced or nacelle drag) cannot be recovered. It is approximated here as $D'_p/D' = 0.5$, based on TASOPT[14] models of relevant aircraft. The power required to energize the boundary layer depends on f_{surf}, the fraction of profile drag dissipation that occurs upstream of boundary layer ingestion. A representative value of $f_{\text{surf}} = 0.9$ is used in the current work.[10,14]

The non-BLI aircraft drag, D', is the summation of nacelle and airframe drag. Nacelle drag is estimated as a function of propulsion stream mass flow, $\dot{m}_i$. Airframe drag is determined from the lift-to-drag ratio of the aero-structural model and the initial aircraft mass, m_{init}.

$$D' = \sum_i D'_{\text{nace},i} + D'_{\text{AF}} \tag{37}$$

$$D'_{\text{nace},i} = r_{\text{nace}}\,\dot{m}_i^{0.7} \tag{38}$$

$$D'_{\text{AF}} = m_{\text{init}}\,g \left(\frac{L}{D'}\right)^{-1}, \tag{39}$$

where $r_{\text{nace}} = 51.9$ kg/s, as correlated to data from TASOPT results.

When propulsors are configured in an array (as with distributed propulsion), the nacelle drag and weight are reduced by a factor of $2/\pi$ since each propulsor only requires a fraction of a full nacelle. This applies to wing BLI and partial fuselage BLI propulsors.

BLI configurations presuppose a degree of integration with the airframe, coupling the aircraft geometry to the aero-propulsive performance. To this end, a propulsion stream's mass flow, $\dot{m}_i$, is split equally among equally-sized $N_{\text{fans},i}$ fans. Fan diameters scale as

$$d_{\text{fan},i} = \sqrt{\kappa \frac{\dot{m}_i}{N_{\text{fans},i}}} \ , \tag{40}$$

where κ characterizes the fan area per unit mass flow, estimated as a function of assumed mission altitude, fan face Mach number, and hub-to-tip ratio, to give values of $\kappa = 36.0$ m^2 s/kg for the thin-haul and $\kappa = 55.5$ m^2 s/kg for larger classes.

The propulsion system must be large enough to ingest the prescribed amount of BLI. This must be reflected in mathematical constraints, in order to capture the trade-off that determines optimal fan size. The amount of BLI drives the propulsor size up, whereas engine drag and weight considerations drive the size down. BLI configurations considered include full fuselage BLI (tail-cone thruster), partial fuselage BLI, and wing BLI (trailing edge propulsors). Constraints for boundary layer height were used to determine wing BLI only.

The boundary layer height is used to determine a lower bound for the wing propulsor diameters, which is calculated as

$$d_{\text{fan}} \geq K_\delta \, c^{6/7}, \tag{41}$$

where c is the wing chord, and $K_\delta = 0.05$ m$^{1/7}$. The right hand side of this equation is derived from the turbulent boundary layer profile over a flat plate.

In addition, the extent of wing BLI is related to the fraction of the span covered by propulsors as $N_{\text{fan}} \, d_{\text{fan}} = (b - d_{\text{fuse}}) \, f_{\text{BLI,wing}}$, where b is the wing span.

D. Technology Assumptions

A major performance driver for electrified aircraft is the mass of the electrical components, which strongly depends on the technology. To consider the effect of technology on electrification, we adopt three distinct technology levels: current, conservative 2035, and optimistic 2035. Here, we present a rationale and values for the specific energy, power, and efficiencies that are used in the present work.

The electrical part of the propulsion system is modeled as a chain of components starting with the energy source (battery) and going all the way to the electrical load (fans). For each electrical fan, an inverter converts the direct current from the battery to alternating current required to power the motor. The motor in turn drives the fan to propel the aircraft. The battery, which works both as an energy and power source, is characterized by a specific energy and a specific power. The inverter and motor are defined by their specific power and efficiency.

Battery specific energy (BSE) is defined as the energy per unit mass. We differentiate between three types of specific energy values: theoretical, cell, and pack. Theoretical BSE, BSE_{th}, is calculated based on electro-chemical reactions and includes only the mass of reactants. Cell BSE, BSE_{cell}, is lower than the theoretical value and obtained from cell manufacturers' specifications: from the nominal voltage, capacity, and mass. It includes the mass of reactants, as well as the mass of all other cell components. The ratio of theoretical to cell and theoretical BSE is the cell efficiency, η_{cell}. For common battery chemistries, η_{cell} is found to be about 28%. Given available data for mature batteries like nickel-cadmium or lead-acid, the cell efficiency is not expected to exceed 40%.

BSE_{cell} is usually quoted in literature as the value of specific energy, but for system-level considerations a more appropriate metric is the pack-level BSE, BSE_{pack}. Battery packs consist of arrays of cells, packaging, wiring, and thermal management systems that contribute to weight. The pack BSE is thus the total *usable* energy provided by a battery pack per unit battery mass, and differs from the cell level BSE by the pack efficiency factor, η_{pack}. Thus,

$$BSE_{\text{pack}} = \eta_{\text{pack}} \, BSE_{\text{cell}} = \eta_{\text{pack}} \, \eta_{\text{cell}} \, BSE_{\text{th}} \ . \tag{42}$$

Based on data from large battery packs used for transportation[f], an average value for η_{pack} is around 70%. In our modeling framework, $E_{\text{bat}}/m_{\text{bat}} = BSE_{\text{pack}}$.

The value of BSE_{pack} that we chose to represent the *current* technology level is estimated at 175 W·h/kg from the lithium-polymer battery of the all-electric Airbus E-Fan.[17] Conservatively, for far term (2035+) applications, this value is expected to rise to 250 W·h/kg, assuming a lithium-nickel-cobalt-aluminum (LNCA) battery with $BSE_{\text{th}} = 740$ W·h/kg and $\eta_{\text{pack}}\,\eta_{\text{cell}} = 0.33$. On the other hand, novel lithium-ion chemistries, like lithium-sulfur (Li-S) and lithium-air (Li-air), have much higher theoretical BSE (2600 W·h/kg and 3500 W·h/kg respectively) and have the potential to achieve substantially higher pack BSE levels. Li-air cells have been demonstrated to reach a BSE of 778 W·h/kg,[18] which translates to a pack value of 540 W·h/kg with a pack efficiency of ∼70%. Assuming development of novel chemistries that mature enough to build commercial rechargeable batteries in the 2035 timeline, the BSE_{pack} can potentially increase to an optimistic value of 900 W·h/kg[g] .

In terms of power, a battery is characterized by the battery specific power (BSP), defined as the maximum power available per unit mass. It is not possible to set BSP without taking into account battery discharge profiles, which vary widely between batteries and their use. We choose instead to fix the ratio of BSE to BSP to the value for NASA's X-57 Maxwell batteries,[19] namely 1200 sec. To account for technological improvements, it is assumed that BSP improves with BSE, while their ratio remains fixed, and so the pack BSP is predicted to reach between 745–2700 W/kg in 2035.

Regarding electrical machines, large motors and generators geared towards aerospace applications are not yet a mature technology. Commercial-off-the-shelf (COTS) motors have specific powers of around 2 kW/kg and are rated for power in the 100 kW range. Motors for large electrified aircraft need to be in the megawatt class. A conservative 2035 estimate for motors predicts specific powers of 9 kW/kg rated at 2 MW.[6] However, NASA is currently funding research geared for aerospace applications with motors rated between 1.0–2.5 MW at specific powers of up to 16 kW/kg,[7] some of which are superconducting, but self-cooled. These levels are expected to be achieved on test-beds in the near term, and will likely decrease when the machines are integrated into aircraft. However, by 2035 it is likely that they will be achieved at system-level. Furthermore, current motors are about 95% efficient, and this efficiency is projected to grow to 98–99% by 2035.[6,7]

A similar rationale can be made for converters and inverters (collectively termed power electronics). Existing power electronics have power and specific power levels of 200 kW and 2.2 kW/kg respectively, and are not geared for aerospace applications. Conservatively, power electronics parameter values are predicted to be 500 kW power and 9 kW/kg specific power in the far term.[6] Based on the projects currently funded by NASA,[7] optimistic estimates are taken at 19 kW/kg rated at 1 MW. Current power electronics are about 95% efficient, and are predicted to reach 98–99% efficiency by 2035.[6,7]

Table 3 summarizes the electrical component parameter values used in the current work, for the three technology levels considered. The numbers presented are for non-superconducting components, or for self-cooled superconducting components. Non self-cooled superconducting elements can potentially yield further weight savings but are not considered for this study.

Table 3: Parameter values for electrical components at three different technology levels.

Parameter	Current	Conservative 2035	Optimistic 2035
Pack BSE (W·h/kg)	175	250	900
Pack BSP (W/kg)	520	745	2700
Motor Specific Power (kW/kg)	2	9	16
Converter Specific Power (kW/kg)	2.2	9	19
Electric Component Efficiency	0.95	0.98	0.99

[f]Boeing 787: $BSE_{\text{cell}} = 102$ W·h/kg, $\eta_{\text{pack}} = 78\%$;[16] Airbus E-Fan: $BSE_{\text{cell}} = 207$ W·h/kg, $\eta_{\text{pack}} = 84\%$;[17] Tesla Model S: $BSE_{\text{cell}} = 266$ W·h/kg, $\eta_{\text{pack}} = 59\%$.

[g]This value is derived assuming a lithium-air-based battery, which gains mass as it discharges and accumulates oxygen, whose mass needs to be accounted for. The theoretical BSE for Li-air of 3500 W·h/kg used to arrive at this number accounts for the added mass of oxygen, in contrast to the 11 000 W·h/kg value sometimes quoted in literature.

Table 4: Baseline aircraft classes that span a variety of passenger capacities and mission ranges.

	Thin-haul	Regional	Medium-haul	Long-haul
Example aircraft	Twin Otter	E175	B737	B777
Design passengers	20	80	180	350
Design range [nmi]	500	1500	3000	6000
Cruise speed [m/s]	77	233	233	249
Span constraint [m]	20	27	36	61
Fuselage diameter [m]	1.83	3.35	3.81	6.19
Fuselage length [m]	15.8	32.0	39.6	73.9
Wing loading [kg/m^2]	146	488	635	684

E. Aircraft Classes

A set of aircraft that span the payload-range space of interest are modeled and analyzed for different electrification levels, different fractions of boundary layer ingestion (BLI), levels of distributed propulsion (DP), and different technology assumptions. As given in Table 4, four different missions are considered: thin-haul (20 passengers, 500 nautical miles range), regional (80 passengers, 1500 nmi), medium haul (180 passengers, 3000 nmi), and long haul (350 passengers, 6000 nmi). These missions are representative of aircraft such as the Viking Air Twin Otter, the Embraer E-175, the Boeing 737, and the Boeing 777 respectively.

Payload and range are fixed for each baseline aircraft and mission, A maximum wing span constraint is set to satisfy airport gate requirements for the respective aircraft classes. Cruise speed, fuselage dimensions, and wing loading are fixed throughout the analysis at the values of the baselines.

F. Limitations of the Approach

Although the unified propulsion system architecture described in Section II.B.1 is valid at any level of fidelity, the analysis framework described in this section and used in the present work is of relatively low fidelity. The main limitation of the framework is that it approximates the mission solely as a cruise segment. As a result, electrification effects during take-off, climb, and descent are not considered. This simplification is likely to more significantly impact the results for short missions, for which take-off and descent make up a significant fraction of the flight time.

In addition, the amount of BLI was not directly optimized within the framework. This was instead specified as an input, and the size and number of propulsors were optimized accordingly, with the implication that their values may not be optimal at some design points. In particular, the results presented in Section III where obtained with the amount of BLI, fan size, and number of propulsors held fixed for all ranges, and better performance may be achievable.

The technology parameter values chosen are based on literature surveys, technical reports, and ongoing NASA-funded research efforts. It is however difficult to predict future developments, and the technology level numbers carry a significant uncertainty. The technology assumptions have a particularly large impact on the feasibility of electrified aircraft that employ batteries (all-electric and hybrid-electric).

Finally, at the level of fidelity at which the present analysis is carried out, configuration-specific layout considerations were not taken into account, in particular those related to the placement of the propulsors and the associated wiring requirements.

We emphasize that the goal of the present work is to carry out a broad (though approximate) trade-space exploration and narrow down the design space to regions where aircraft electrification shows the most potential. As such, the development of the framework focused on capturing the most fundamental trends and trade-offs.

III. Results

The framework is now applied to explore the design space with the goal of determining the particular missions where electrification has the most potential. We start by varying the range, and show that there is

an optimal propulsion architecture for a given range. The individual effects of technology, BLI and DP are then illustrated. Finally, some point designs are presented to highlight the attributes of electrified aircraft.

A. Mission and Best Architecture

For this section, we use the following two aircraft baseline sets with optimistic 2035 technology, as summarized in Table 5. A turbo-electric set has $f_S = 0$, $f_L = 1$, and $f_{\mathrm{BLI}_E} = 0.5$. An all-electric set has $f_S = 1$ and $f_{\mathrm{BLI}_E} = 0.5$. Each class has a different number and size of fans, and for the turbo-electric set, a different level of BLI for the mechanical fans. These were set to give the best performance at the design range of each class, as discussed in Section III.D.

Note that the designs show massively distributed propulsion (DP) with a large number of small fans. These were chosen to look at trends with and without DP, as discussed in Section III.C. These designs are not necessarily desirable from a commercial point of view. Also, due to the limitations of this low-fidelity analysis, some configuration-specific DP issues like placement of propulsors are not considered.

1. Range

In order to determine the effect that range has on performance for the various aircraft classes considered, we start from the turbo-electric aircraft set and allow the source electrification factor, f_S, to be optimized. Figure 5 shows the optimal source electrification factor, f_S, versus range for the four aircraft classes, and the productivity-specific energy consumption, $PSEC$, benefit relative to a conventional architecture. It shows that the optimum level of electrification and propulsion system architecture depends strongly on the mission. At low ranges, f_S optimizes to 1 and an all-electric architecture provides the lowest $PSEC$, with a maximum of 50% benefit relative to a conventional architecture for the thin-haul, and around 40% for the other classes.

For ranges above around 800 nmi, the turbo-electric architecture is best (f_S optimizes to 0), even though the $PSEC$ benefit is only on the order of 7%. Hybrid-electric aircraft might find a niche at intermediate ranges. Adding a turbo-generator to an all-electric aircraft can act as as a range extender, allowing it to travel longer distances while still being more energy-efficient than a conventional aircraft. Note that here only series turbo-electric architectures were considered.

Although the $PSEC$ benefit plateaus at high ranges with $f_L = 1$, if the load electrification factor is free to change, the benefits of electrification actually increases with range. Figure 6 shows the $PSEC$ benefit for a partial turbo-electric architecture with $f_L \approx 0.5$, *i.e.* with roughly equal propulsive flow power coming from electrical and mechanical fans. Each line represents a different class, and so the corresponding airplanes are actually very different in size even if though they fly the same range. It is interesting to note that the curves for all but the smallest class nearly collapse at low ranges (1000 nmi and under). Given the limitations of our models, an upper range limit was set to the design range for the class.

2. Payload

To investigate the sensitivity of energy requirement to payload variations, thin-haul aircraft were flown with different numbers of passengers: 20 (design capacity), 17, and 14 passengers. The curves in Fig. 7 show the effect of payload changes on $PSEC$ versus range for all-electric and turbo-electric architectures. $PSEC$ is mostly insensitive to payload, except at the smallest and largest ranges for an all-electric architecture. This

Table 5: Aircraft baselines for mission analysis.

	Turbo-electric ($f_S = 0$)							All-electric ($f_S, f_L = 1$)		
	f_L	Mechanical Fans			Electrical Fans			Electrical Fans		
		N_{fan_M}	d_{fan}[m]	f_{BLI_M}	N_{fan_E}	d_{fan}[m]	f_{BLI_E}	N_{fan_E}	d_{fan}[m]	f_{BLI_E}
Thin-haul	1	NA	NA	NA	254	0.071	0.5	146	0.122	0.5
Regional	0.55	2	0.79	0.2	248	0.097	0.5	98	0.246	0.5
Medium-haul	0.48	2	1.14	0.2	308	0.104	0.5	94	0.343	0.5
Long-haul	0.43	2	2.18	0.2	298	0.185	0.5	118	0.464	0.5

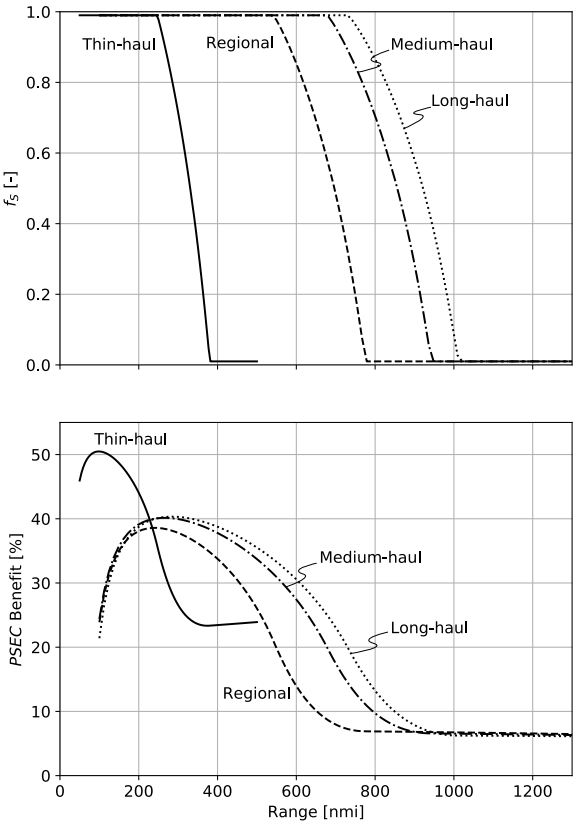

Figure 5: Relative PSEC benefit for turboelectric aircraft at short ranges for all classes; BSE = 900 W·h/kg, $[P/m]_{\text{mot}}$ = 16 kW/kg, $[P/m]_{\text{conv}}$ = 19 kW/kg, f_{BLI_E} = 0.5, f_L = 1; thin-haul with N_{fan_E} = 254, d_{fan_E} = 0.071 m; regional with N_{fan_E} = 248, d_{fan_E} = 0.097 m; medium-haul with N_{fan_E} = 308, d_{fan_E} = 0.104 m; long-haul with N_{fan_E} = 298, d_{fan_E} = 0.185 m.

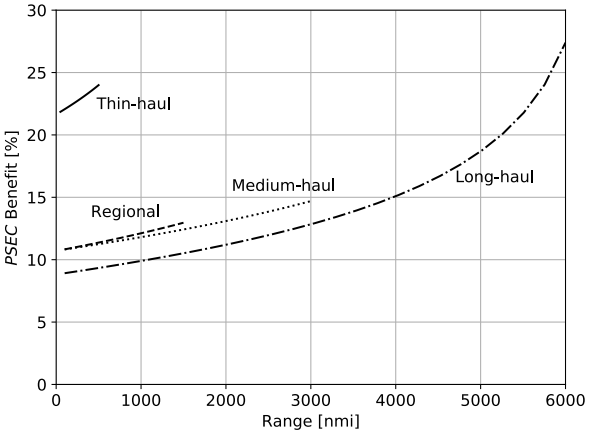

Figure 6: Relative PSEC benefit for turboelectric aircraft at long ranges for all classes; BSE = 900 W·h/kg, $[P/m]_{\text{mot}}$ = 16 kW/kg, $[P/m]_{\text{conv}}$ = 19 kW/kg, f_{BLI_E} = 0.5; thin-haul with $f_L = 1$, $f_{\text{BLI}_M} = 0$; regional with $f_L = 0.55$, f_{BLI_M} = 0.2; medium-haul with f_L = 0.48, $f_{\text{BLI}_M} = 0.2$; long-haul with $f_L = 0.43$, f_{BLI_M} = 0.2; N_{fan_E} and d_{fan_E} as in Fig. 5 for all classes.

is an indication that the incremental energy required to transport each extra passenger is roughly constant. Similar results were observed with conservative 2035 technology and for larger classes.

The largest effect of payload on $PSEC$ is seen for the all-electric case at its maximum feasible range of 300 nmi. Here, the reduction in energy requirement outweighs the reduction in productivity, such that $PSEC$ decreases. A 30% reduction in payload results in a 30% decrease in PSEC at this range.

B. Electric Component Technologies

This section looks at the effect of technology parameters on the feasibility and performance of electrified aircraft. The objective is to quantify the benefits as technology levels improve. All-electric aircraft are feasible only at reduced ranges for all sizes, as will be shown in Section III.D. Therefore, to show the effect of parameters that define an electrical propulsion system, a reduced-range thin-haul aircraft is chosen and the technology parameters are varied while keeping other factors constant.

For this analysis, the baseline conventional aircraft carries 20 passengers over a reduced range of 100 nmi. It is assumed to be powered by two mechanically driven fans, and further, assumed to ingest no fraction of the boundary layer ($f_S = 0$, $f_L = 0$, and $f_{\text{BLI}_M} = 0$). The all-electric aircraft ($f_S = 1$ and $f_L = 1$) also flies the same mission, at different technology levels. It is assumed that electrification enables distributed propulsion (DP) and boundary layer ingestion (BLI). Battery effects (BSE and BSP) and other component

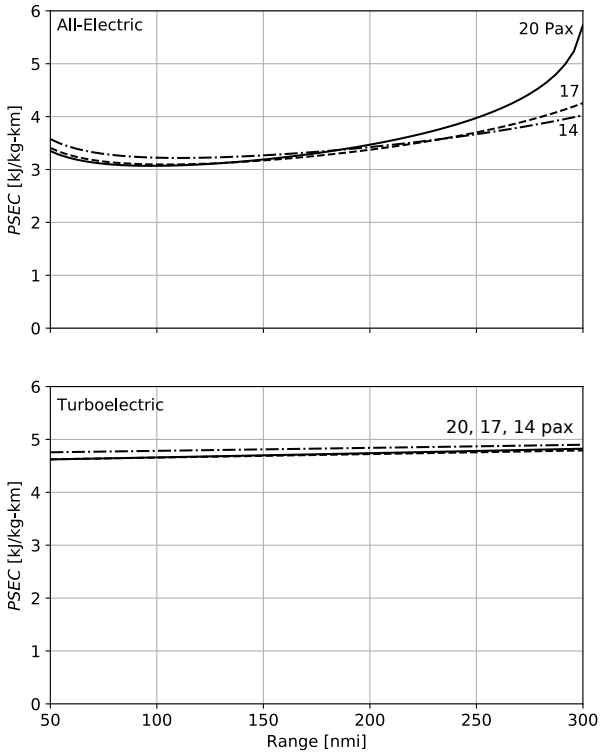

Figure 7: Effect of payload on $PSEC$ versus range for all- and turbo-electric thin-haul aircraft; BSE = 900 W·h/kg, $[P/m]_{\text{mot}} = 16\,\text{kW/kg}$, $[P/m]_{\text{conv}} = 19\,\text{kW/kg}$, $f_{\text{BLI}_E} = 0.5$; all-electric with $N_{\text{fan}_E} = 146$, $d_{\text{fan}_E} = 0.122\,\text{m}$; turbo-electric with $f_L = 1$, $N_{\text{fan}_E} = 254$, $d_{\text{fan}_E} = 0.071\,\text{m}$.

effects (specific powers of motors and converters) are considered separately. When one set of parameters is varied, the remaining technology parameters are set to be at the optimistic 2035 values from Section II.D.

1. Effects of Battery Technology

For a reduced-range 100 nmi mission, the all-electric aircraft is not feasible at current and conservative 2035 battery technology. Figure 8 shows the effect of increasing BSE (and with it, BSP) on the productivity-specific energy consumption ($PSEC$) metric. The conventional aircraft has a constant $PSEC$ as BSE varies, as it is powered by hydrocarbon fuel and thus carries no batteries. In terms of configuration, the closest all-electric aircraft has 2 electric fans and no BLI. When the BSE is under 350 W·h/kg, this all-electric aircraft is infeasible. Between 350–400 W·h/kg, the all-electric aircraft becomes feasible, but it requires more energy than the conventional. As BSE increases further, the battery mass to carry the mission energy decreases, and leads to a sharp drop in the $PSEC$. At optimistic 2035 battery technology, the all-electric aircraft consumes about 37% less energy than the conventional aircraft. At even higher BSE values, the $PSEC$ curve flattens out. This is due to the battery mass increasingly becoming a smaller fraction of the aircraft takeoff mass. Further increases in BSE provide diminishing benefits in energy consumption. The initial sharp drop also shows that the $PSEC$ is sensitive to changes in BSE.

Figure 8 also shows the range of propulsor configurations available for the all-electric aircraft by varying the number of fans and BLI. At optimistic 2035 battery technology, the all-electric aircraft with 2 fans and no BLI consumes less energy than the conventional baseline. When the design space is opened up to include massive distribution of fans and BLI, the benefits are twofold: (i) the aircraft becomes feasible at smaller BSE values, and (ii) it offers even greater $PSEC$ reduction at a given BSE value. It can also be seen that all-electric aircraft are feasible at reduced ranges within the predicted BSE numbers. Furthermore, they provide a $PSEC$ benefit over conventional aircraft, and this benefit increases with DP and BLI.

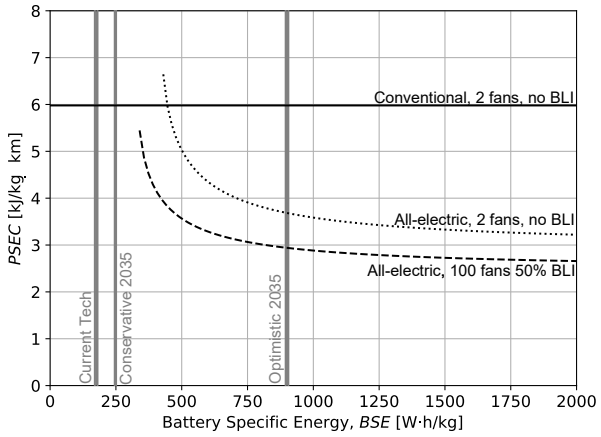

Figure 8: Effect of battery technology on $PSEC$ with DP and BLI for 100 nmi all-electric thin-haul aircraft; $[P/m]_{\text{mot}} = 16\,\text{kW/kg}$, $[P/m]_{\text{conv}} = 19\,\text{kW/kg}$, $f_S = 1$, $f_L = 1$.

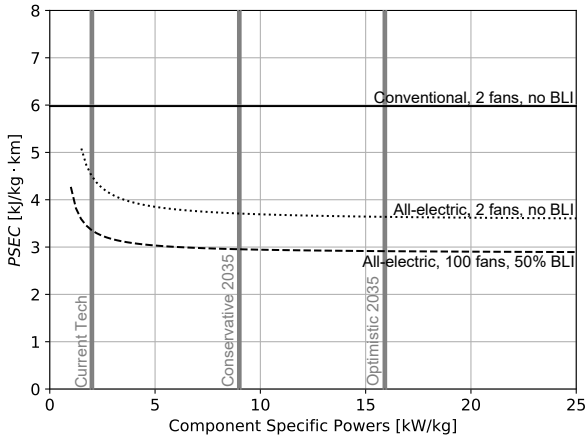

Figure 9: Effect of component specific powers on $PSEC$ with DP and BLI for 100 nmi all-electric thin-haul aircraft; $BSE = 900$ W·h/kg, $f_S = 1$, $f_L = 1$.

2. Effects of Component Specific Powers

Figure 9 shows the effects of increasing component (motors and inverter) specific powers on $PSEC$. All-electric aircraft are feasible and beneficial over conventional aircraft even with current technology (although BSE and BSP are still set to optimistic 2035 values). Again, the conventional aircraft has a constant $PSEC$ as component specific powers improve, since it does not carry any converters or motors. For the all-electric aircraft, $PSEC$ improves as specific powers increase. Even with 2 electric fans, current technology already provides a benefit of about 25% over conventional. At conservative and optimistic 2035 values, this benefit increases to 28% and 30% respectively.

Figure 9 also shows the effect of DP and BLI on $PSEC$. At conservative 2035 values, an all-electric aircraft with 2 fans and no BLI offers a $PSEC$ reduction of about 42% over conventional, which increases to 48% with 100 fans and 50% BLI. Little benefit is obtained for values higher than 8 kW/kg since the components' mass make up an increasingly smaller fraction of the aircraft takeoff mass. The flattened $PSEC$ curve also suggests that the metric is less sensitive to component specific powers than it is to battery technology, This indicates that the obstacles for a feasible all-electric aircraft lie with battery technology, rather than with motors and converters.

Following this conclusion, a turbo-electric architecture (no batteries) could be feasible even with current technology. Figure 10 demonstrates this, here for a larger medium-haul aircraft designed to carry 180 passengers over 3000 nmi. The conventional aircraft has two mechanically driven fans with no BLI and a $PSEC$ of about 4.2 kJ/kg·km. The turbo-electric aircraft has 308 electrically distributed fans, ingesting 20% of the total boundary layer over the fuselage and 50% over the wing.

Even with current technology, the turbo-electric aircraft has a $PSEC$ benefit of 7% over the conventional. This advantage increases to 16% with conservative 2035 technology and to 19% with optimistic 2035 technology. Thus, while all-electric aircraft may be infeasible for longer missions, turbo-electrics are feasible for longer missions. This was demonstrated here for the medium-haul, but was found to be true for all classes.

C. Specific Effects of BLI and DP

1. Boundary Layer Ingestion

Some of the effects due to BLI have already been seen in Section III.B. It is, however, also useful to point out the effects on mission. Figure 11 shows the $PSEC$ and takeoff mass for an all-electric thin-haul aircraft plotted versus range for the optimistic 2035 technology assumptions. Results are shown for no BLI, 25% and 50% BLI. Note that where the lines terminate, the model is infeasible and cannot close. It can be seen that

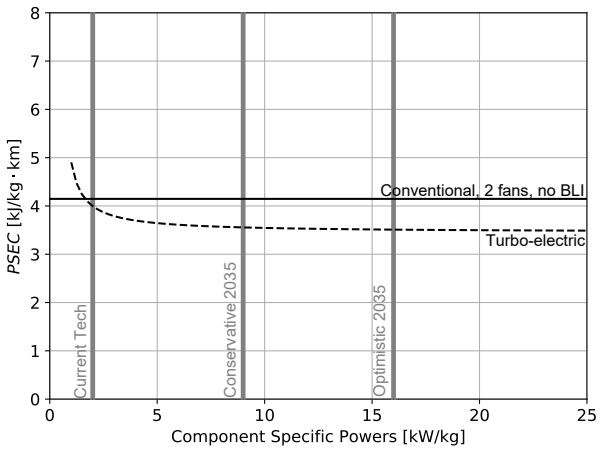

Figure 10: Effect of improving component specific powers on PSEC for a medium-haul aircraft; turbo-electric: $f_L = 0.48$, $f_{\text{BLI}_M} = 0.2$, $N_{\text{fan}_M} = 2$, $d_{\text{fan}_M} = 1.14\,\text{m}$, $f_{\text{BLI}_E} = 0.5$, $N_{\text{fan}_E} = 308$, $d_{\text{fan}_E} = 0.104\,\text{m}$.

the effect of BLI is both to increase the feasible range of the aircraft and to reduce the $PSEC$ for a given range. The extent of weight growth due to electrification is also reduced. These observations also hold for the larger aircraft classes considered.

BLI can thus be seen as a technology that is both facilitated by electrification, and that enhances the beneficial effects thereof.

2. Distributed Propulsion

Considering that electrification enables distributed propulsion (DP), the reduced-range all-electric thin-haul aircraft from Section III.B becomes more beneficial with a greater number of smaller-diameter fans. DP provides two benefits, as shown in Fig. 12: first, the all-electric aircraft with more fans starts to become feasible at lower BSE values. Second, it provides a larger $PSEC$ reduction at a given BSE value. For example, with 20 fans, the all-electric aircraft sees a PSEC reduction compared to the conventional, whereas with 2 fans, it has a $PSEC$ disadvantage. At optimistic 2035 battery technology, the 20-fan all-electric aircraft provides a $PSEC$ benefit of about 40% over the conventional. However, as with increasing BSE, increasing DP has diminishing returns: going from 20 fans to 100 fans provides less benefits than going from 2 to 20.

D. Point Performance Comparisons

1. Aircraft Configurations

Since the design space of electrified aircraft is large, it is useful to define the concept of a *configuration* as the minimum set of inputs needed to assess aircraft performance. A configuration (i) consolidates discrete assumptions, and (ii) samples a region of the design space by converging to the optimum within the specified range of parameters. Thus, spanning the electrified design space simplifies to spanning a reduced configuration space of discrete inputs. Table 6 presents architecture classifications that further summarize the electrified configuration space. In this section, only the optimistic 2035 technology assumptions were used.

It should be noted that here, an advanced conventional aircraft was also considered, which can take advantage of some BLI but not distribution. The baseline classes are then evaluated under these classifications, with the $PSEC$-minimizing propulsion system architectures shown in Table 6. For the electrified systems, it was found that the turbo-electric thin-haul class favors the fully turbo-electric configuration, with all flow power coming from electrically powered fans, whereas the larger classes favor partial turbo-electric, where some of the flow power comes from conventional turbine-powered fans. These configurations serve as points of departure, and are used to define the baseline aircraft defined in Table 5.

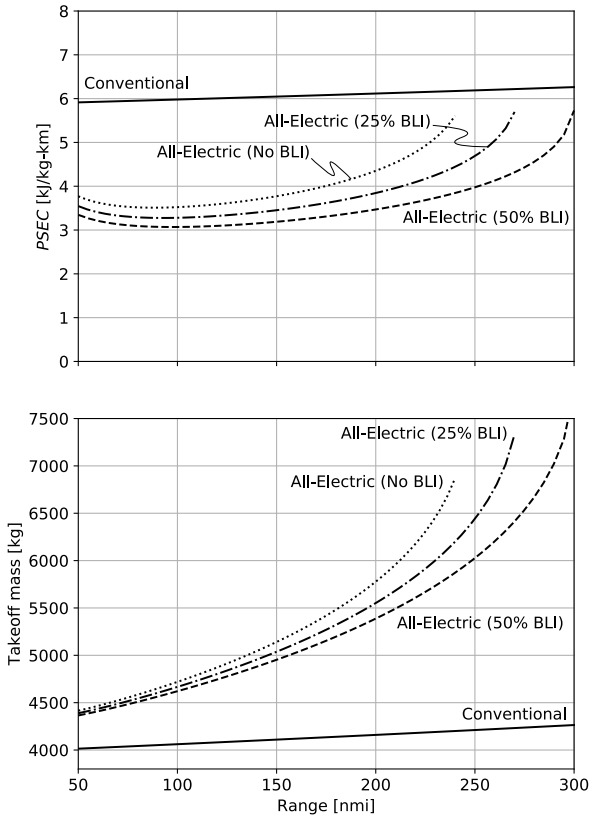

Figure 11: Effect of BLI on PSEC and takeoff mass versus range for all-electric thin-haul aircraft; BSE = 900 W·h/kg, $[P/m]_{\text{mot}}$ = 16 kW/kg, $[P/m]_{\text{conv}}$ = 19 kW/kg, $f_S = 1$, $f_L = 1$, $N_{\text{fan}_E} = 146$, $d_{\text{fan}_E} = 0.122$ m.

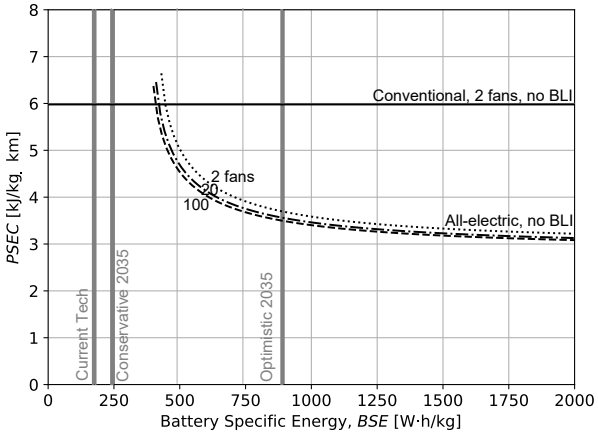

Figure 12: Effect of distributed propulsion on PSEC versus BSE for a 100 nmi all-electric thin-haul aircraft; $[P/m]_{\text{mot}}$ = 16 kW/kg, $[P/m]_{\text{conv}}$ = 19 kW/kg, $f_S = 1$, $f_L = 1$, $f_{\text{BLI}_E} = 0$.

2. Design- and Reduced-Range Performance

The minimum-$PSEC$ configurations were compared to each other, both at the baseline aircraft design ranges, and at reduced ranges where the all-electrics are feasible. Fig. 13 presents the PSEC reductions for each class at the design range of the baseline aircraft. It can be seen that the advanced conventional aircraft offer PSEC reductions between about 12% and 22% compared to current conventional aircraft at design ranges. Turbo-electrics offer slightly higher reductions: between 13% and 27%. The all-electric configuration is infeasible for all classes at this range: the battery mass required to power the flight is larger than the airframe parameters

Table 6: Architecture Classification

Architecture classification	**Description**	**Selected configuration**
Conventional (Baseline)	Turbofans only	Two podded turbofans
Advanced Conventional	BLI turbofans, no distribution	Two embedded turbofans, 40% fuselage BLI.
Turbo-electric	Turbofans or turbo-generators powering electrical fans BLI and electrical distribution possible	Thin-haul: fully turbo-electric with wing BLI Larger classes: Partial turbo-electric with wing BLI Two turbofans with generators, 40% fuselage BLI
All-electric	Battery-powered electrical fans BLI and distribution possible	Fully turbo-electric with wing BLI

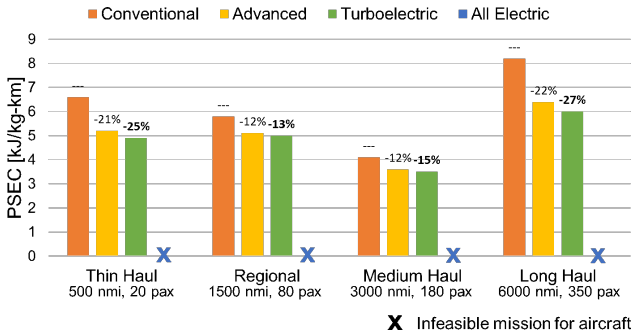

Figure 13: Aircraft $PSEC$ at baseline design range for optimistic 2035 technology assumptions.

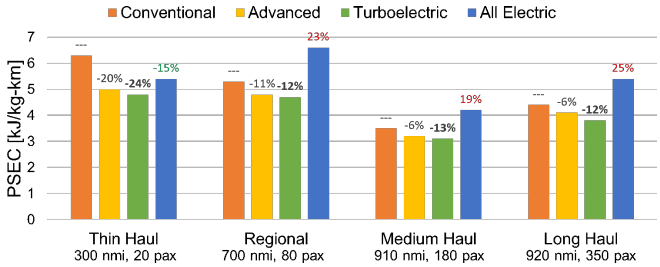

Figure 14: Aircraft $PSEC$ at reduced range for optimistic 2035 technology assumptions.

can support.

The design ranges were then reduced to the maximum range at which the all-electric configurations are feasible. It was found that for the thin-haul, regional, medium- and long-haul these ranges are 300, 700, 910 and 920 nmi respectively. The $PSEC$ values at this range for the various classes are shown in Fig. 14

Here, the all-electric decreases $PSEC$ by 15% at a reduced thin-haul mission, but offers no benefit for the longer missions. Advanced and turbo-electric aircraft still demonstrate significant performance improvements, though the benefits have decreased; it was observed in Section III.A that the $PSEC$ benefit increases with range for partial turbo-electric aircraft.

Both trends are the result of the logarithmic nature of the range equation. Although fuel is recursively needed to carry fuel mass, the aircraft gets lighter throughout the mission, requiring less power; battery-powered flight does not share this advantage. This discrepancy grows with mission fuel and range, resulting in poorer all-electric performance for longer missions.

It should be noted here that the reduced range at which the all-electric aircraft is feasible is a rather arbitrary design point to judge the performance benefit of electrification. As was shown in Section III.A, reducing range further leads to large efficiency benefits for all classes considered.

IV. Summary and Conclusions

This paper presents a unified framework and analysis for aircraft with both conventional and electrified propulsion systems. The approach allows for comparison of the on-board energy requirement of aircraft with various propulsion system architectures, including conventional hydrocarbon-based, all-electric, turbo-electric, and hybrid-electric. The architecture parameterization as source and load electrification factors forms a unified view of the propulsion system that encompasses all the various architectures. While the analysis presented is low-fidelity and based on the cruise segment, it captures the major trends and trade-offs of electrification at cruise, including the effects of technology, distributed propulsion, and boundary layer ingestion.

The exploration of the design space shows areas where electrified aircraft show an energy consumption benefit over conventional aircraft. Configuration changes allow for the highest potential to be reached, and inclusion of distributed propulsion (DP) and boundary layer ingestion (BLI) expands the feasible range for electrified aircraft while offering energy benefits. Electrification enables easier distribution of fans that are

then able to ingest a larger fraction of the wing and/or fuselage boundary layer. Multiple smaller fans also provide weight benefits compared to fewer larger fans, further reducing energy consumption.

In terms of propulsion system architectures, the much lower specific energy of batteries compared to hydrocarbon fuel is a barrier to all-electric aircraft adoption. All-electric aircraft are feasible only for short ranges (under 1000 nmi), for all classes considered, even with optimistic battery technology predictions. However, for the missions for which they are feasible, all-electrics might offer significant energy benefits over conventional aircraft.

Apart from waiting for battery technology to improve, other avenues to electrification are possible with hybrid- and turbo-electric architectures. Turbo-generators added to all-electric aircraft (resulting in a hybrid-electric architecture) can act as range extenders, offering energy consumption benefits over conventional aircraft at higher ranges than what is possible with all-electrics. Hybrid-electrics occupy a niche for mid-size missions. At larger ranges, eliminating the battery entirely with a turbo-electric architecture results in configurations with the highest energy consumption benefit.

Turbo-electric aircraft take advantage of the high specific energy of hydrocarbon fuel and leverage other benefits related to electrification (DP and BLI). It was found that current motor and power electronics technology levels make turbo-electric architectures feasible. The energy consumption decreases with technology improvements, but there is an upper limit to the benefits as lighter components make up smaller and smaller fractions of the propulsion system mass. In particular, the energy benefit of fully turbo-electric architectures, in which thrust is produced entirely by electric fans, plateaus at higher ranges. On the other hand, if the turbo-generators are also connected to fans (in a partial turbo-electric architecture), the energy benefit increases quite substantially with range.

Thus, different electrified propulsion system architectures have different optimal applications, and electrified aircraft appear to be beneficial as long as they target the appropriate mission.

Acknowledgments

This work was supported by NASA under a Leading Edge Aeronautics Research for NASA (LEARN3) Project, through NASA/MIT Collaborative Agreement NNX16AK25A. We are thankful for the support and guidance provided by Ralph Jansen and Raymond Beach from NASA Glenn Research Center. The research benefited from the collaboration with Aurora Flight Sciences as a partner in the project, and from the direction provided by Edward Greitzer of MIT as the Principal Investigator.

References

[1]Moore, M. D. and Fredericks, B., "Misconceptions of electric propulsion aircraft and their emergent aviation markets," American Institute of Aeronautics and Astronautics, 2014.

[2]Welstead, J. and Felder, J., "Conceptual Design of a Single-Aisle Turboelectric Commercial Transport with Fuselage Boundary Layer Ingestion," *54th AIAA Aerospace Sciences Meeting*.

[3]Antcliff, K., Guynn, M., T.V, M., Wells, D., Schneider, S., and Tong, M., "Mission Analysis and Aircraft Sizing of a Hybrid-Electric Regional Aircraft," *SciTech 2016*.

[4]Isikveren, A. T., Pornet, C., Vratny, P. C., and Schmidt, M., "Optimization of Commercial Aircraft Using Battery-Based Voltaic-Joule/Brayton Propulsion," *Journal of Aircraft*.

[5]Hepperle, M., "Electric Flight-Potential and Limitations," .

[6]The National Academies of Sciences, Engineering, and Medicine, "Commercial Aircraft Propulsion and Energy Systems Research: Reducing Global Carbon Emissions," , 2016.

[7]Jansen, R. H., Bowman, C., Jankovsky, A., Dyson, R., and Felder, J., "Overview of NASA Electrified Aircraft Propulsion Research for Large Subsonic Transports," *53rd AIAA/ SAE/ ASEE Joint Propulsion Conference*.

[8]Uranga, A., Drela, M., Greitzer, E., Hall, D., Titchener, N., Lieu, M., Siu, N., Huang, A., Gatlin, G., and Hannon, J., "Boundary Layer Ingestion Benefit of the D8 Aircraft," *AIAA Journal*, Vol. 55, No. 11, 2017, pp. 3693–3708, doi:10.2514/1.J055755.

[9]Smith, L., "Wake Ingestion Propulsion Benefit," *Journal of Propulsion and Power*, Vol. 9, No. 1, 1993, pp. 74–82, doi:10.2514/3.11487.

[10]Hall, D. K., Huang, A. C., Uranga, A., Greitzer, E. M., Drela, M., and Sato, S., "Boundary Layer Ingestion Propulsion Benefit for Transport Aircraft," *Journal of Propulsion and Power*, Vol. 33, No. 5, 2017, pp. 1118–1129, doi:10.2514/1.B36321.

[11]Drela, M., "Power balance in aerodynamic flows," *AIAA journal*, Vol. 47, No. 7, 2009, pp. 1761–1771.

[12]Burnell, E. and Hoburg, W., "GPkit software for geometric programming," `https://github.com/convexengineering/gpkit`, 2018. Version 0.7.0.

[13]Raymer, D. P., *Aircraft Design: A Conceptual Approach (AIAA Education Series) 5th Edition*, American Institute of Aeronautics and Astronautics (AIAA), 2012.

[14]Drela, M., "TASOPT 2.00 Transport Aircraft System OPTimization: Technical Description," `http://web.mit.edu/drela/Public/N+3/TASOPT_doc.pdf`, 2010. Accessed: 05/08/2018.

[15]Kuhn, H. and Sizmann, A., *Fundamental prerequisites for electric flying*, Deutsche Gesellschaft für Luft-und Raumfahrt-Lilienthal-Oberth eV, 2012.

[16]Kolly, J. M., Panagiotou, J., Czech, B. A., and NTSB, "The Investigation of a Lithium-Ion Battery Fire Onboard a Boeing 787 by the US National Transportation Safety Board," , 2013.

[17]Airbus Group, "E-Fan The New Way to Fly," `http://www.airbusgroup.com/service/mediacenter/download/uuid=48b1bd2c-a428-4c65-82e5-ed3e923bd142`, 2015. Accessed: 07/26/2016.

[18]Zhang, T., Imanishi, N., Shimonishi, Y., Hirano, A., and Takeda, Y., "A novel high energy density rechargeable lithium/air battery," *Chemical Communications*, Vol. 46, 2010, pp. 1661–1663.

[19]Gibbs, Y. and NASA, "NASA Armstrong Fact Sheet: NASA X-57 Maxwell," `https://www.nasa.gov/centers/armstrong/news/FactSheets/FS-109.html`, 2017. Accessed: 05/07/2018.